LA-4770-MS

CMB-13 Research on Carbon and Graphite

Report No. 17

Summary of Progress from February 1, 1971 to April 30, 1971

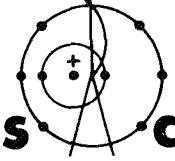

los alamos
scientific laboratory
of the University of California
LOS ALAMOS, NEW MEXICO 87544

UNITED STATES
ATOMIC ENERGY COMMISSION
CONTRACT W-7405-ENG. 36

This LA. . .MS report presents the summary of progress of CMB-13 research on carbon and graphite at LASL. The four most recent Summary of Progress Reports in this series, all unclassified, are:

LA-4480-MS	LA-4631-MS
LA-4526-MS	LA-4714-MS

This report, like other special-purpose documents in the LA. . .MS series, has not been reviewed or verified for accuracy in the interest of prompt distribution.

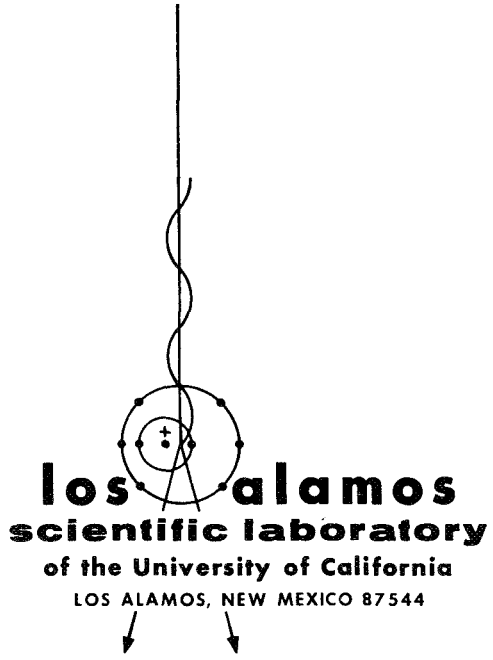

LA-4770-MS
SPECIAL DISTRIBUTION
ISSUED: September 1971

CMB-13 Research on Carbon and Graphite

Report No. 17

Summary of Progress from February 1, 1971 to April 30, 1971*

by

Morton C. Smith

*Supported in part by the Office of Advanced Research and Technology of the National Aeronautics and Space Administration.

CMB-13 RESEARCH ON CARBON AND GRAPHITE
REPORT NO. 17: SUMMARY OF PROGRESS FROM FEBRUARY 1, 1971 TO APRIL 30, 1971

by

Morton C. Smith

I. INTRODUCTION

This is the seventeenth in a series of progress reports devoted to carbon and graphite research in LASL Group CMB-13, and summarizes work done during the months of February, March, and April, 1971. It should be understood that in such a progress report many of the data are preliminary, incomplete, and subject to correction, and many of the opinions and conclusions are tentative and subject to change. This report is intended only to provide up-to-date background information to those who are interested in the materials and programs described in it, and should not be quoted or used as a reference publicly or in print.

Research and development on carbon and graphite were undertaken by CMB-13 primarily to increase understanding of their properties and behavior as engineering materials, to improve the raw materials and processes used in their manufacture, and to learn how to produce them with consistent, predictable, useful combinations of properties. The approach taken is microstructural, based on study and characterization of natural, commercial, and experimental carbons and graphites by such techniques as x-ray diffraction, electron and optical microscopy, and porosimetry. Physical and mechanical properties are measured as functions of formulation, treatment, and environmental variables, and correlations are sought among properties and structures. Raw materials and manufacturing techniques are investigated, improved, and varied systematically in an effort to create specific internal structures believed to be responsible for desirable combinations of properties. Prompt feedback of information among these activities then makes possible progress in all of them toward their common goal of understanding and improving manufactured carbons and graphites.

Since its beginning, this research has been sponsored by the Division of Space Nuclear Systems of the United States Atomic Energy Commission, through the Space Nuclear Propulsion Office. More recently additional general support for it has been provided by the Office of Advanced Research and Technology of the National Aeronautics and Space Administration. Many of its facilities and services have been furnished by the Division of Military Application of AEC. The direct and indirect support and the guidance and encouragement of these agencies of the United States Government are gratefully acknowledged.

II. SANTA MARIA COKE

A. Previous Work

Santa Maria coke and the nearly isotropic graphites made from it have previously been discussed in Reports 9 through 16 in this series.

B. Effects of Heat-Treatment (J. M. Dickinson)

The effects of calcining temperature on the properties of molded graphites made from calcined Santa Maria coke were described in Report No. 15. Small samples of Lot C-15 Santa Maria coke, which had been heat-treated to 1470, 1840, and 2170°C after grinding, were on hand from that experiment, and have since been used to make the extruded graphites listed in Table I.

TABLE I

MANUFACTURING CONDITIONS, EXTRUDED SANTA MARIA GRAPHITES

Specimen Number	Filler Calcining Temp., °C	Binder Conc., pph	Extrusion Conditions: Pressure, psi	Velocity, in./min	Mix, °C	Chamber, °C	Vacuum, μ	Green dia, in.
ADA 1	1470	28.5	4050	171	36	45	300	.501
ADA 2	1840	28	4275	164	37	50	500	.5005
ADA 3	2170	27	4725	167	36	45	450	.5015

Varcum 8251 furfuryl alcohol resin was used as the binder and all graphites were extruded as 0.5-in.-dia rods under the conditions summarized in the table. Normal heat-treating procedures were used.

All rods contained visible cracks after curing. At least in part, this was due to use of an excess of binder; all mixes were somewhat wet. However, not enough filler material was available to repeat the extrusions.

In spite of the cracks, all three graphites had good densities and normal Young's moduli--which are listed in Table II. The graphites made from the two fillers heat-treated at the higher temperatures had significantly higher densities than did that made from the filler calcined at 1470°C.

C. Lot G-35 Flour (J. M. Dickinson)

Santa Maria Lot G-35 graphite flour was prepared at the Y-12 Plant of Union Carbide Corporation, and is identified by them as a "Blend No. 1" grind which has been graphitized at 2500°C. In Reports 15 and 16 in this series, it has been described and compared with a previous shipment of Blend No. 1 flour (CMB-13 Lot G-26). The Lot G-35 material is significantly finer than the Lot G-26 flour, although the two are otherwise very similar.

The fabrication behavior of Lot G-35 was investigated by using it as the principal filler material in the manufacture of the extruded graphites listed in Table III. In all cases it was mixed with Thermax carbon black in the proportion 85 parts graphite flour to 15 parts carbon black. Two different furfuryl alcohol resin binders were used: Varcum 8251 and QX247 (which is discussed later in this report under "Binders"). Specimens ADB1 and ADB2 were 0.5-in.-dia rods; specimens ADB4 and ADB5 were tubes 0.25-in. o.d. and 0.10-in. i.d. To reduce resin viscosity and assist mixing, the QX247 binder was diluted with acetone in the case of specimen ADB4. One result of the use of acetone was a significant reduction in extrusion pressure.

Curing, baking, and graphitizing were done in normal cycles.

Properties of the finished graphites are listed in Table IV. Densities of the rods were very high, especially for specimen ADB2, made with the higher-viscosity QX247 resin. Densities of the tubes were lower, as would be expected from their geometry, although densities were not as low as those of tubes previously made from the Lot G-26 filler. The use of acetone as a mixing aid resulted in significant increases in bulk density, carbon residue, electrical conductivity, and Young's modulus. (The use of acetone for this purpose is further discussed in a later section of this report, under "Binders.")

Although it differs significantly in mean particle size and particle-size distribution from the previous "Blend No. 1" graphite flour, Lot G-35 appears to be a good Santa Maria filler, and is well suited for use in the manufacture

TABLE II

PROPERTIES OF EXTRUDED SANTA MARIA GRAPHITES

Specimen Number	Bulk Density, g/cm^3	Binder Carbon Residue, %	Young's Modulus, (a) 10^6 psi
ADA 1	1.876 ± .003	46.5 ± .4	1.90 ± .01
ADA 2	1.897 ± .005	46.6 ± .3	1.90 ± .02
ADA 3	1.894 ± .002	47.5 ± .4	1.87 ± .01

(a) With-grain.

TABLE III

MANUFACTURING CONDITIONS, EXTRUDED GRAPHITES MADE WITH LOT G-35 FLOUR

Specimen Number	Shape	Binder		Extrusion Conditions					Green Dia., in.
		Type	Conc., pph	Pressure, psi	Velocity, in./min	Mix, °C	Chamber, °C	Vacuum, μ	
ADB1	Rod [a]	V8251	26	4500	164	42	45	350	0.5035
ADB2	Rod [a]	QX247	26	8100	156	45	35	375	0.5035
ADB4									
Tubes 1-8	Tube [b]	QX247	27 [c]	16,470	200	46	43	450	0.252
Tubes 9-16	Tube [b]	QX247	27 [c]	18,000	300	--	--	---	0.252
Tubes 17-24	Tube [b]	QX247	27 [c]	16,240	189	--	--	---	0.252
Tubes 25-30	Tube [b]	QX247	27 [c]	15,525	111	--	--	---	0.252
ADB5									
Tubes 1-8	Tube [b]	QX247	27	19,350	138	53	43	450	0.252
Tubes 9-16	Tube [b]	QX247	27	22,275	180	--	--	---	0.252
Tubes 17-24	Tube [b]	QX247	27	22,275	138	--	--	---	0.252
Tubes 25-30	Tube [b]	QX247	27	22,500	120	--	--	---	0.252

(a) Rod 0.5-in. dia.

(b) Tube 0.25-in. OD, 0.10-in. ID.

(c) Plus 15 ml acetone.

TABLE IV

PROPERTIES OF EXTRUDED GRAPHITES MADE WITH LOT G-35 FLOUR

Specimen Number	Bulk Density, g/cm^3	Binder Carbon Residue, %	Electrical Resistivity, [a] μΩ cm	Young's Modulus, [a] 10^6 psi
ADB1	1.905	47.0 ± .3	1693 ± 25	1.80 ± .02
ADB2	1.915	49.3 ± .4	1625 ± 14	1.85 ± .02
ADB4				
Tubes 1-8	1.861	43.6 ± .2	1833 ± 16	1.68 ± .007
Tubes 9-16	1.834	42.7 ± .9	1866 ± 51	1.60 ± .02
Tubes 17-24	1.847	42.2 ± .4	1877 ± 18	1.62 ± .007
Tubes 25-30	1.848	41.4 ± .3	1879 ± 28	1.62 ± .02
Average	1.849 ± .012	40.5 ± .9	1864 ± 26	1.63 ± .03
ADB5				
Tubes 1-8	1.833	41.3 ± .6	1890 ± 15	1.55 ± .02
Tubes 9-16	1.827	41.4 ± 1.1	1878 ± 10	1.56 ± .02
Tubes 17-24	1.822	39.8 ± .6	1901 ± 7	1.54 ± .004
Tubes 25-30	1.822	39.7 ± .6	1935 ± 33	1.52 ± .01
Average	1.827 ± .007	40.6 ± 1.1	1902 ± 30	1.55 ± .02

(a) With-grain.

TABLE V

COMPOSITION AND DENSITY DATA FOR HOT-MOLDED NATURAL GRAPHITES

Specimen Number	Mix Composition, [a] Parts by Wt.	Calculated Binder Optimum, pph	Binder Residue % (Baked)	Density, g/cm^3 Packed Filler (Baked)	Density, g/cm^3 Bulk Baked	Density, g/cm^3 Bulk Graph.	Dimensional Change, Baked to Graphitized, % $\Delta \ell$	Δ d	Δ v
75A-1b	100 G-21 + 18 PP-4	14.8	58.6	1.812	2.004	1.892	+2.4	+0.1	+2.7
59H	95 G-21 + 5 TP-4 + 18 PP-3	17.2	55.4	1.743	1.918	1.844	+0.9	+0.0	+1.0
59J	90 G-21 + 10 TP-4 + 20 PP-3	19.0	59.7	1.692	1.894	1.838	+0.2	-0.0	+0.2
59K	85 G-21 + 15 TP-4 + 22 PP-3	21.4	68.8	1.630	1.876	1.831	+0.1	-0.1	-0.2
59D, L	80 G-21 + 20 TP-4 + 22 PP-3	21.6	63.2	1.615	1.858	1.821	-0.6	-0.2	-1.1
59E	75 G-21 + 25 TP-4 + 25 PP-3	22.6	55.5	1.586	1.817	1.805	-1.3	-0.3	-2.0
59F, M	70 G-21 + 30 TP-4 + 28 PP-3	26.3	58.9	1.510	1.764	1.768	-1.4	-0.6	-2.6
75B-1	100 G-34 + 14 PP-4	12.3	58.1	1.876	2.035	1.892	+2.7	+0.2	+3.1
75D-2b	90 G-34 + 10 TP-4 + 12 PP-4	11.4	57.4	1.872	2.001	1.883	+1.6	+0.1	+1.9
75D-3	85 G-34 + 15 TP-4 + 12 PP-4	13.1	72.9	1.815	1.974	1.882	+1.0	-0.0	+0.9
75D-4	80 G-34 + 20 TP-4 + 12 PP-4	11.1	72.5	1.852	2.013	1.867	+0.4	+1.7	+3.9
75D-5	75 G-34 + 25 TP-4 + 14 PP-4	14.9	70.0	1.746	1.917	1.855	+0.3	-0.3	-0.3
75F-1	99.5 G-34 + 0.5 T-3 + 11 PP-4	10.8	65.3	1.916	2.054	1.924	+2.3	+0.2	+2.7
75F-2	99.0 G-34 + 1 T-3 + 11.5 PP-4	11.4	71.6	1.894	2.058	1.922	+2.1	+0.1	+2.3
75F-3	98.0 G-34 + 2 T-3 + 12 PP-4	11.7	68.5	1.878	2.032	1.911	+2.1	+0.1	+2.4
75E-1	100 G-34 + 14 PP-4	11.5	51.9	1.898	2.036	1.884	+3.0	+0.2	+3.3
75E-2	100 G-34 + 0.5 Kynol + 14 PP-4	9.5 [b]	35.1	1.952	2.052	1.898	+3.3	+0.2	+3.6
75E-3	100 G-34 + 0.5 CFA + 14 PP-4	10.0	37.4	1.938	2.040	1.876	+3.2	+0.3	+3.7
75E-4	100 G-34 + 0.5 GFA + 14 PP-4	10.5	28.7	1.924	2.002	1.863	+2.6	+0.2	+3.0

(a) Mix Components:

- G-21 ---Fine natural graphite.
- G-34 ---Coarse natural graphite.
- TP-4 ---Thermax carbon black.
- T-3 ---Carbolac 1 carbon black.
- PP-3, -4 ---Barrett 30 MH pitch.
- Kynol ---Phenolic fibers.
- CFA ---Carbon fibers.
- GFA ---Graphite fibers.

(b) Includes Kynol residue.

of extruded graphites. As is discussed in a later section of this report, it also appears promising as a raw material for the manufacture of graphite-matrix composites.

TABLE VI

PROPERTIES OF HOT-MOLDED GRAPHITES MADE FROM FILLER G-34 WITH ADDITIONS OF VARIOUS FIBERS

SPECIMEN NO:	75 E-1	75 E-2	75 E-3	75 E-4
Fiber in mix	None	Kynol	CFA	GFA
Density, g/cm^3	1.884	1.898	1.876	1.863
Flexure Str., psi				
With-grain	3008	3072	2820	2960
Across-grain	771	717	675	814
Resistivity, $\mu\Omega$ cm				
With-grain	508	508	473	524
Across-grain	2880	4303	3728	2723
Therm. Cond., W/cm-°C				
With-grain	2.41	2.31	2.67	2.27
Across-grain	0.44	0.39	0.41	0.49
Anisotropies				
BAF[(a)]	2.84	3.66	3.13	3.05
M-Factor[(b)]	6.1	6.8	7.8	6.9
Flexure Str.	3.90	4.28	4.18	3.64
Resistivity	5.67	8.46	7.88	5.19
Therm. Cond.	5.48	5.93	6.73	4.63

(a) Bacon Anisotropy Factor, σ_{oz}/σ_{ox}.

(b) Exponent of cosine in cosine function which best represents angular distribution of intensities of reflected x rays.

III. HIGHLY ORIENTED POLYCRYSTALLINE GRAPHITES

A. Previous Work

The continuing development of highly anisotropic manufactured graphites has been discussed in Reports 7, 8, 10-12, and 16 in this series. Recent work has been concerned principally with the effects of various filler additives on the properties of hot-molded, pitch-bonded graphites made with natural graphite fillers. Four series of graphites have been made, which are listed in Table V. These represent various combinations of two natural graphite fillers, two grades of carbon black, and three types of fibers. The two fillers were a very fine grade of natural flake graphite (CMB-13 Lot G-21), and a somewhat coarser grade of the same material (CMB-13 Lot G-34) both of which have been described in Report 16. The two carbon blacks were Thermax and Carbolac 1. The three fibers were Kynol, an uncarbonized phenolic fiber; CFA, a carbon fiber; and GFA, a graphite fiber.

B. Effect of Fiber Type (R. J. Imprescia)

The four graphites of Series 75E were made from the coarser natural graphite filler (Lot G-34) with Barrett 30MH coal-tar pitch binder. Specimen 75E-1 contained no fiber addition. Specimens 75E-2, 75E-3, and 75E-4 each contained 0.5% of fiber, the fibers being Kynol, CFA, and GFA, respectively, in the three specimens. All fibers were cut to a nominal 0.25-in. length by the manufacturer.

Kynol is an uncarbonized phenolic fiber produced by The Carborundum Co. at a nominal diameter of 14 μ, and has been described in Report 12. CFA and GFA are carbon and graphite fibers, respectively, produced by HITCO at nominal diameters of 0.000,3 in. (7.6 μ) from a rayon fiber precursor. CFA is carbonized by heating

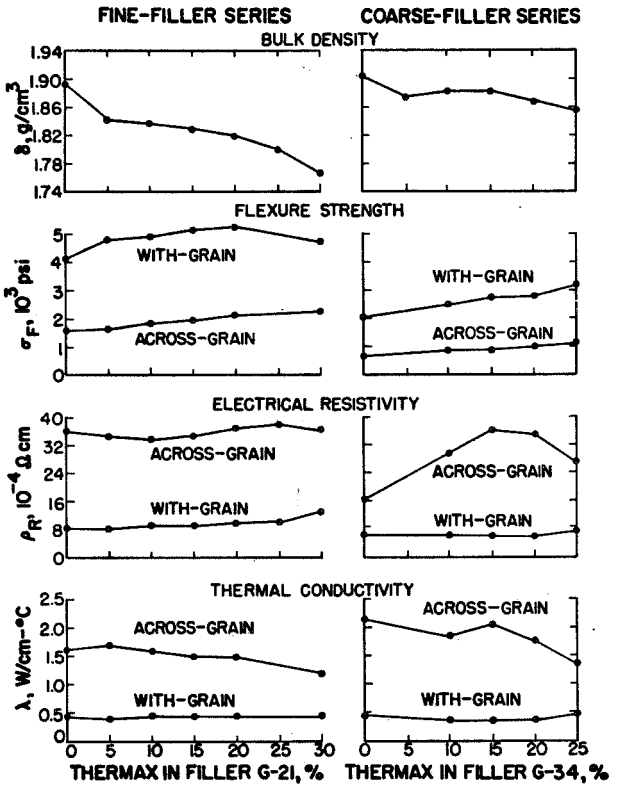

Fig. 1. Effects of Thermax additions on the properties of molded, pitch-bonded graphites made from very fine (Lot G-21) and coarser (Lot G-34) natural graphite fillers.

the rayon to 2000°F (1093°C). GFA is graphitized by heating it to 4000°F (2204°C).

The raw mixes for molding were prepared by a standard solvent-blending technique using tetrahydrofuran, and were vacuum-dried. Because of the fragility of the carbon and graphite fibers, the food-chopping step was omitted. Specimens were hot-molded by "Program A" and graphitized at about 2750°C in flowing argon.

Properties of these graphites are listed in Table VI. At least in the small concentrations used for this experiment, none of the fiber additions had a large effect on the properties of the finished graphites. Both Kynol and CFA did significantly increase across-grain electrical resistivity, and both appeared to increase the general anisotropy of the graphite.

C. Effects of Thermax Additions (R. J. Imprescia)

Two series of graphites were made in which the main variable was the proportion of Thermax carbon black added to the raw mix. In the first of these (graphite 75A and the Series 59 specimens) the principal filler was the very fine natural graphite, Lot G-21. In the second (75B and the 75D series) the principal filler was the coarser natural graphite, Lot G-34. In both cases the binder used was Barrett 30MH coal-tar pitch, which was combined with the filler and carbon black by standard solvent-blending and hot food-chopping. Specimens were hot-molded at 4000 psi and 900°C by "Program A", and were graphitized at approximately 2800°C in flowing helium or argon.

Properties of these graphites are summarized in Table VII and plotted in Fig. 1. For both fillers, bulk densities were decreased by the Thermax additions. However, with the coarser fillers densities were higher and were less affected by the carbon black. Flexure strength in both with-grain and across-grain orientations increased with Thermax concentration. Maximum across-grain strength in both cases was at the highest Thermax concentrations used, and was 2262 psi at 30% Thermax in the fine filler and only 1118 psi at 25% Thermax in the coarse filler.

In the fine-filler series, electrical resistivity in the across-grain direction was nearly constant at about 3600 μΩcm, and in the with-grain direction increased slowly with Thermax concentration from 838 μΩcm without Thermax to 1294 μΩcm at 30% Thermax. In the coarse-filler series, across-grain resistivity reached a maximum of 3601 μΩcm at 15% Thermax; in the with-grain direction it remained nearly constant at about 640 μΩcm.

Across-grain thermal conductivities were nearly constant for both series, at about 0.4 W/cm-°C. In the with-grain direction thermal conductivity decreased with increasing Thermax concentration, from about 1.6 to 1.2 W/cm-°C for the fine-filler series and from about 2.1 to 1.4 W/cm-°C for the coarse-filler series.

TABLE VII

PROPERTIES OF HOT-MOLDED NATURAL GRAPHITE FILLERS WITH THERMAX ADDITIONS

	Fine Filler (G-21)							Coarse Filler (G-34)					
SPECIMEN NO:	75A-1b	59H	59J	59K	59D, L	59E	59F, M	75B-1	75D-1	75D-2b	75D-3	75D-4	75D-5
Thermax, %	0	5	10	15	20	25	30	0	5	10	15	20	25
Density, g/cm^3	1.892	1.844	1.838	1.831	1.821	1.805	1.768	1.903	1.875	1.883	1.882	1.867	1.855
Flexure Str., psi													
With-grain	4142	4807	4963	5140	5266	---	4734	2044	---	2510	2755	2809	3143
Across-grain	1600	1644	1871	1968	2126	---	2262	652	---	878	876	995	1118
Resistivity, μΩcm													
With-grain	838	842	907	901	965	987	1294	631	---	615	582	613	743
Across-grain	3608	3489	3341	3470	3680	3784	3653	1649	---	2963	3601	3522	2676
Therm. Cond. [a]													
With-grain	1.63	1.69	1.58	1.50	1.49	---	1.20	2.14	---	1.85	2.06	1.77	1.36
Across-grain	0.45	0.40	0.45	0.43	0.43	---	0.46	0.44	---	0.37	0.36	0.37	0.47
Anisotropies													
BAF [b]	3.10	2.82	2.85	2.78	2.56	2.18	1.72	2.78	---	3.31	2.48	2.76	2.10
M-Factor [c]	5.0	5.3	5.0	5.3	5.2	4.2	3.4	4.3	---	6.2	6.0	5.7	4.4
Flexure Str.	2.59	2.92	2.65	2.61	2.48	---	2.09	3.14	---	2.86	3.14	2.82	2.81
Resistivity	4.31	4.14	3.68	3.85	3.81	3.83	2.82	2.61	---	4.82	6.19	5.75	3.60
Therm. Cond.	3.62	4.22	3.51	3.49	3.47	---	2.61	4.86	---	5.00	6.08	4.78	2.89

(a) W/cm-°C.

(b) Bacon Anisotropy Factor, σ_{oz}/σ_{ox}.

(c) Exponent of cosine in cosine function which best represents angular distribution of intensities of reflected x rays.

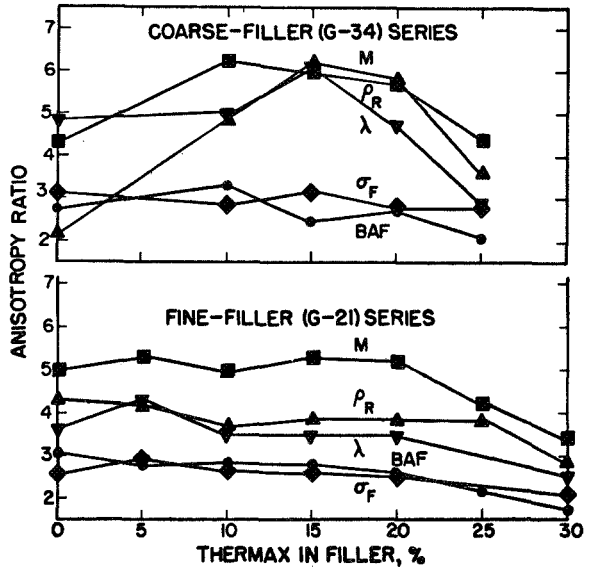

Fig. 2. Anisotropies of molded graphites as functions of Thermax additions to coarse and fine natural graphite fillers.

Anisotropies of these graphites are plotted in Fig. 2 as functions of Thermax concentration. They were generally higher for graphites made from the coarser filler, with no consistent trend but perhaps with a tendency to peak in the range 10 to 20% Thermax. For the fine-filler series anisotropies were nearly constant with Thermax additions up to 20%, then decreased with larger Thermax additions.

D. Effects of Carbolac 1 Additions (R. J. Imprescia)

Three specimens of the 75F series, listed in Table V, were made with the coarser (Lot G-34) natural graphite filler containing small additions of Carbolac 1 carbon black (CMB-13 Lot T-3).

Carbolac 1 is a very fine carbon black produced by the Cabot Corporation, with an average particle size of 0.000, 9 μ, and was described in Report 7 in this series. It is very fluffy and difficult to handle during certain

TABLE VIII

PROPERTIES OF HOT-MOLDED GRAPHITES MADE FROM FILLER G-34

WITH CARBOLAC 1 ADDITIONS

SPECIMEN NO:	75 B-1	75 F-1	75 F-2	75 F-3
Carbolac 1 in Filler, %	0	0.5	1	2
Density, g/cm^3	1.903	1.924	1.922	1.911
Flexure Str., psi				
With-grain	2044	2674	2646	2494
Across-grain	652	829	848	927
Resistivity, μΩcm				
With-grain	631	638	561	627
Across-grain	1649	2835	2745	3349
Therm. Cond., W/cm-°C				
With-grain	2.14	1.97	1.76	1.75
Across-grain	0.44	0.40	0.64	0.51
Anisotropies				
BAF[(a)]	2.78	2.35	2.99	3.02
M-Factor[(b)]	4.3	4.2	4.8	5.2
Flexure Str.	3.14	3.23	3.12	2.69
Resistivity	2.61	5.54	4.89	5.34
Therm. Cond.	4.86	4.93	2.75	3.43

(a) Bacon Anisotropy Factor, σ_{oz}/σ_{ox}.

(b) Exponent of cosine in cosine function which best represents angular distribution of intensities of reflected x rays.

blending operations, so that only small quantities were added to the filler. The concentrations used were 0.5, 1, and 2%. These were mixed with the natural graphite filler and Barrett 30MH coal-tar pitch using standard solvent-blending and hot food-chopping methods. The specimens were hot-molded using "Program A" and were graphitized in flowing argon to about 2800°C.

Properties of the graphitized specimens are listed in Table VIII. Bulk densities in all cases were greater than 1.9 g/cm^3. There was no obvious effect of the small carbon black additions on density.

The first small (0.5%) addition of Carbolac 1 significantly increased flexure strengths in both with-grain and across-grain orientations. Larger additions continued to increase across-grain strength, while with-grain strength remained nearly constant at about 2600 psi.

Across-grain strengths were quite low, but it may be significant that strength in this orientation was increased almost 50% by a carbon-black addition of only 2%. With the same filler, about 20% of Thermax was required to produce a similar increase in strength.

With-grain electrical resistivity remained nearly constant at about 600 μΩcm. Across-grain resistivity increased rapidly with Carbolac 1 concentration, from 1649 μΩcm without Carbolac to 3349 μΩcm at 2% Carbolac.

Thermal conductivity in the with-grain direction decreased significantly with increasing Carbolac concentration, from an initial 2.14 W/cm-°C to a final 1.75 W/cm-°C at 2% Carbolac. In the across-grain direction, conductivity increased slightly with Carbolac concentration.

TABLE IX

COMPOSITIONS AND EXTRUSION CONDITIONS FOR ADG COMPOSITES

Specimen Number	Vol. % ZrC	Extrusion Conditions: Pressure, psi	Velocity, in./min	Temperature, °C: Mix	Chamber	Vacuum, Torr	Green Dia, in.	Comments
ADG 8	0	4050	164	46	47	500	.505	Cracks.
ADG 6	2	4860	164	44	40	500	.505	Excess-binder cracks.
ADG 5	10	4140	160	46	43	500	.505	Excess-binder cracks.
ADG 4	17	4140	160	46	45	500	.505	Excess-binder cracks.
ADG 3	23	3960	164	40	40	500	.505	Excess-binder cracks.
ADG 2	23	3960	157	43	45	500	.504	Excess-binder cracks.
ADG 7	29	4050	164	43	43	500	.506	Slight excess binder. OK.
ADG 10	29	5400	164	40	42	1000	.506	OK.
ADG 11	30	5400	164	43	43	1000	.506	OK.
ADG 12	30	6840	164	45	44	1000	.503	Tube. OK.

Anisotropies were high for all properties measured, but showed no consistent trend with Carbolac 1 concentration.

IV. GRAPHITE-CARBIDE COMPOSITES

A. Previous Work

Investigations of the production and properties of graphite-matrix composites containing dispersed ZrC particles have previously been discussed in Reports 14-16 in this series.

B. Extruded Graphite-ZrC Composites (J. M. Dickinson)

The ADG series of composites listed in Tables IX and X was made to explore the effects of ZrC additions to isotropic, high-expansion graphites. The principal filler used was the minus 200 mesh fraction screened from Lot G-35 Santa Maria graphite flour, discussed above. The ZrC powder used was obtained from LASL Group CMB-6, and was identified by them as Lot 77D. The binder was Varcum 8251 furfuryl alcohol resin catalyzed with 4% maleic anhydride.

In all of the early extrusions in this series (Specimens ADG 1 through ADG 8) binder contents were somewhat too high, and some of the rods produced contained cracks. In many cases the cracks were not serious, and good properties measurements could be made. From Table X it is evident that very low electrical resistivities are possible with composites of this type together with relatively high elastic moduli and strengths. Electrical-resistivity measurements indicated reasonable uniformity in the last few extrusions of the series in which binder concentration was about right, although earlier specimens were not uniform.

Specimen ADG 8, which contained no carbide, was exceptional for a graphite made with Varcum 8251 binder. Its density, 1.924 g/cm^3, was as high as those usually obtained using furfuryl alcohol resins of much higher viscosity, and essentially no variation in electrical resistivity could be detected from point to point and rod to rod.

Composites of high quality and interesting properties can be made using the -200 mesh Lot G-35 Santa Maria flour. Binder content is critical, and must be determined experimentally for each composition desired.

Particle packing in this system is discussed in a later section of this report.

V. RAW MATERIALS

A. Commercial Graphite Flours (H. D. Lewis)

Samples from three new lots of Airco-Speer KX-88 ("Nuclear No. 2") graphite flour have been obtained from LASL Group CMB-6. They are identified as BBL60-1, BBL60-2, and BBL60-3, and in Table XI their particle

TABLE X

PROPERTIES OF ADG GRAPHITES

Specimen Number	Vol. % ZrC	Bulk Density, g/cm^3	Binder Carbon Residue, %	Electrical Resistivity, $\mu\Omega$ cm	Young's Modulus, 10^6 psi	Compressive Strength, psi
ADG 8	0	1.924	47	1740	1.8	---
ADG 6	2	1.957	44	1640	1.8	---
ADG 5	10	2.311	43	810	2.5	---
ADG 4	17	2.661	41	430	3.5	---
ADG 3	23	2.935	40	315	4.4	---
ADG 2	23	2.928	41	310	4.4	---
ADG 7	29	3.222	40	220	5.9	---
ADG 10	29	3.215	40	210	6.0	---
ADG 11	30	3.239	40	270	6.2	39800
ADG 12	30	3.276	42	190	6.5	---

characteristics are compared with those of an earlier lot described in Report No. 16. The three new lots were found to be essentially the same, and to be slightly finer than the previous lot, with a little more surface-connected porosity. However, differences between the new and old lots were small, and could have resulted simply from sampling variations. All samples contained a relatively large fraction of material coarser than 60 μ, and none was well represented with regard to particle-size distribution by the lognormal approximation.

A sample of Airco-Speer JM-15 graphite flour, also obtained from LASL Group CMB-6, was found to be quite similar in particle-size distribution to the KX-88 samples. However, as is indicated by the characterization data of Table XI, it was a somewhat coarser powder with less surface-connected porosity.

Great Lakes 1076-MX graphite flour, again from CMB-6, was slightly finer than either the KX-88 or the JM-15 flour, with surface-connected porosity approximately equal to that of JM-15. Its characterization parameters are also listed in Table XI.

B. Lump Cokes (H. D. Lewis)

Screen-analysis data were used to calculate interval-model sample statistics for the three lump cokes listed in Table XI. These calculations were made primarily to estimate the specific surface areas of the cokes prior to grinding, as a basis for evaluating their relative grindabilities.

C. Grinding Products (H. D. Lewis)

Also listed in Table XI are the particle characteristics of three grinding products now being used to manufacture hot-molded graphites. Of these, GP-16 is the product of grinding a needle coke (CMB-13 Lot CNL-1) and both G-33 and G-34 are ground natural graphites. Because of large differences in shape between the more acicular needle-coke and the very flaky natural-graphite particles, data for these two types of material are only qualitatively comparable with each other and with data for nonneedle and isotropic flours.

Of the two natural graphites, Sample G-34 was the coarser but had the higher fuzziness ratio (which is the ratio of measured to calculated specific surface area). This probably results not only from the presence of more surface-connected porosity but also from fraying of particle edges, which has been observed to occur with natural graphites under certain grinding conditions.

TABLE XI

PARTICLE CHARACTERISTICS

Sample	Helium Density, g/cm³	Micromerograph Statistics[a] $\bar{d}_3$, Mean Dia, μ	$s^2_{d_3}$, Sample Variance	S_W, (Calc.) cm²/g[b]	CV_d[c]	BET Data S_W, (BET) cm²/g	d_s,[d] μ	R_F, Fuzziness Ratio[e]
KX-88[f]	2.172	33.50	339	1946	1.11	87,200	0.320	44.8
KX-88, BBL60-1	2.181	32.86	310	1863	1.05	92,500	0.297	49.7
KX-88, BBL60-2	2.180	32.23	307	1941	1.05	94,600	0.291	48.8
KX-88, BBL60-3	2.182	31.83	302	1912	1.12	95,000	0.290	49.7
JM-15	2.185	39.48	362	1572	1.12	78,200	0.351	39.7
1076-MX	2.199	31.44	946	3510	0.90	127,500	0.214	36.3
Needle Coke, Lump	---	5157[g]	---	6.8[g]	---	---	---	---
Needle Coke, Green	---	4704[g]	---	9.5[g]	---	---	---	---
Isotropic Coke, Calcined	---	4344[g]	---	8.3[g]	---	---	---	---
GP-16	2.190	13.51	102.5	3983	0.98	87,900	0.31	22.1
G-33	2.280	12.74	57.8	3548	0.99	64,800	0.41	18.3
G-34	2.280	26.27	196.7	1842	1.00	46,800	0.56	25.4

(a) Interval model.

(b) Specific surface area.

(c) Coefficient of variation.

(d) $d_s = 6/\rho S_W$.

(e) S_W (BET) ÷ S_W (Calc.).

(f) Previously reported (Report 16).

(g) From screen analysis.

D. Quaker Oats Resins (E. M. Wewerka, J. M. Dickinson)

Four new experimental furfuryl alcohol resins and an experimental curing catalyst have been received from the Quaker Oats Co. and are now being evaluated. These are:

QX 261: An experimental furfuryl alcohol resin, with viscosity of 1600 cp, that is virtually free of monomer. Gel-permeation chromatography ("GPC") suggests that this resin was made simply by distilling most of the monomer from a resin of lower viscosity.

QX 262: An experimental furfuryl alcohol resin said to be rich in a grainy-appearing, butter-like substance, whose isolation from such resins has occasionally been reported in the literature. It has been speculated that this substance is either a very high-molecular-weight polymer, possibly cross-linked, or a low-molecular-weight material in the form of a cyclic product. Such a material has been separated in CMB-13 by centrifugation of furfuryl alcohol resins, but has not been studied further.

GPC indicates only that resin QX 262 contains a large amount of monomer, with perhaps less material than usual in the mid-molecular-weight range.

QX 263: A furfuryl alcohol resin with viscosity of 2400 cp which has been modified chemically to introduce a greater degree of aromatic character into the basic

TABLE XII

MOLECULAR DISTRIBUTIONS OF THREE CMB-13 FURFURYL ALCOHOL RESINS

Identification	Viscosity, cp	Proportion of Resin in Each Distribution Region, %				Sample Statistics			
		Region 1	Region 2	Region 3	Region 4	Mean	Variance	Skewness	Coefficient of Variation
EMW 314	275	14.9	40.1	35.6	9.4	2.40	0.73	+.038	0.356
EMW 322	590	12.9	39.0	38.6	9.5	2.45	0.70	-.005	0.341
EMW 316-317	1020	10.9	39.5	39.4	10.2	2.49	0.68	-0.002	0.331

resin molecules. GPC shows that the basic furfuryl alcohol resin structure is retained, but the chromatogram indicates the presence of extraneous material at both the high and the low ends of the molecular-size distributions.

QX 265: A furfuryl alcohol resin similar to QX 263 but of higher viscosity (11,000 cp) and chemically modified to a lesser degree. GPC indicates some enhancement of the furfuryl alcohol resin structure in the dimer, trimer, and tetramer regions.

QX 260: A liquid curing catalyst claimed by Quaker Oats chemists to increase carbon yields from furfuryl alcohol resins. It is reported to have low toxicity and an indefinite shelf life at room temperature, to cause no precuring reactions in resin-catalyst mixtures at or below room temperature, and to cause curing to occur at about 125°C. Because of its low viscosity and apparently high solubility, QX 260 at about 5% concentration appears to mix well with furfuryl alcohol resins.

The monomer-free binder, QX 261, was used to produce an extruded graphite ("ADL 1"). During mixing the material was extruded from the food-chopper as chips or powder rather than the usual spaghetti. The mix appeared to be drier than usual and the extrusion pressure was somewhat higher than normal--presumably because the lubricating effect of the monomer was absent. With a normal curing cycle, the extruded rods cracked. A slower cure (2.5°C/hr) reduced cracking and increased density (from 1.897 to 1.908 g/cm^3). Properties of the finished graphite were not quite as good as those of similar graphites made with CMB-13 ("EMW") resins of equivalent viscosity, but were superior to those of most graphites made with low-viscosity furfuryl alcohol resins.

E. CMB-13 Resins (J. M. Dickinson, E. M. Wewerka)

The three experimental binders listed in Table XII were synthesized specifically to satisfy the criteria, discussed in previous reports, which we believe identify a good furfuryl alcohol resin for use as a binder in the manufacture of extruded graphites. The descriptions in Table XII are of the type discussed in Report No. 8 in this series. In each case the gel-permeation chromatogram of the resin has been arbitrarily divided into four sequentially numbered regions representing fractions having progressively larger mean molecular sizes and the sample statistics describe the distribution of material among these regions. All three of these binders have nearly symmetrical molecular-size distributions and satisfy the requirement that more than 70% of the distribution should fall in regions 2 and 3. Their viscosities cover a broad range, and the ability to synthesize a variety of resins of controlled viscosity, each of which has a narrow molecular-size distribution and a moderately large mean molecular size, represents an important accomplishment.

These three binders were used to manufacture the extruded graphites listed in Tables XIII and XIV. Either Lot G-26 Santa Maria or Lot G-18 Great Lakes 1008-S graphite flour was used as the principal filler, together with 15 parts of Thermax carbon black to 85 parts of the graphite flour. With the G-26 filler, binder concentration was 25 pph; with the G-18 filler it was 27 pph. Manufacturing conditions were normal, and the mixes were

TABLE XIII

COMPOSITION AND EXTRUSION CONDITIONS FOR GRAPHITES MADE WITH THE BINDERS OF TABLE XII

Specimen Number	Filler Used	Binder Used		Extrusion Conditions				
		Identification	Viscosity cp	Pressure, psi	Velocity, in./min	Temperature, °C		Vacuum, Torr
						Mix	Chamber	
ADE 1	G-26	EMW 314	275	5940	164	38	53	600
ADE 3	G-26	EMW 314	275	4275	164	44	44	500
ADE 2	G-18	EMW 314	275	5130	171	34	42.5	700
ADJ 1	G-26	EMW 322	590	5320	171	44	47	<1000
ADJ 2	G-18	EMW 322	590	5310	164	43	43	<1000
ADF 1	G-18	EMW 316-317	1020	6210	164	48	40	400
ADF 2 (a)	G-26	EMW 316-317	1020	6120	171	55	46	500
ADF 3	G-26	EMW 316-317	1020	6840	164	46	40	500

(a) Cracked because of excess binder.

TABLE XIV

PROPERTIES OF GRAPHITES MADE FROM BINDERS OF TABLE XII

Specimen Number	Bulk Density, g/cm^3	Binder Carbon Residue, %	Electrical Resistivity, $\mu\Omega$ cm	Young's Modulus, 10^6 psi	Compressive Strength, psi
ADE 1	1.900 ± 0.004	49.8 ± 0.2	1662 ± 23	1.75 ± 0.03	17900
ADE 3	1.903 ± 0.001	48.9 ± 0.3	1615 ± 13	1.73 ± 0.01	18200
ADE 2	1.886 ± 0.002	48.0 ± 0.3	1169 ± 3	2.46 ± 0.01	11100
ADJ 1	1.910 ± 0.001	49.4 ± 0.1	1542 ± 8	1.77 ± 0.01	16350
ADJ 2	1.899 ± 0.004	47.9 ± 0.1	1087 ± 3	2.03 ± 0.06	11400
ADF 1	1.912 ± 0.002	49.0 ± 0.1	1129 ± 6	2.63 ± 0.01	13300
ADF 2	1.912 ± 0.002	51.6 ± 0.3	1671 ± 16	1.80 ± 0.02	-----
ADF 3	1.916 ± 0.003	50.1 ± 0.3	1614 ± 11	1.83 ± 0.03	19400

extruded as 0.5-in.-dia rods, which were finally graphitized at about 2800°C. Graphite ADF2 contained an excess of binder (26.5 pph) and cracked during processing. All other samples appeared sound.

With the exception of ADF2, these were excellent graphites. Densities above 1.90 g/cm^3 were attained with both the Santa Maria and the Great Lakes fillers, and were uniformly higher than when commercial Varcum 8251 binder has been used under similar conditions. Resin EMW 314, a low-viscosity resin similar to Varcum 8251 except in molecular-size distribution, gave good graphites with both fillers, but particularly with the Santa Maria filler. Graphite ADE3 is a duplicate of ADE1, made a month later to see if the properties of the latter were reproduced. They were.

The ADJ graphites may be particularly interesting, since their properties are good and binder viscosity was low enough (590 cp) to make fabrication procedures very easy.

Compressive strengths, especially of graphites made with the Santa Maria filler, are very high for unimpregnated, unmodified graphites.

In general, use of these tailored binders had the expected result of producing superior extruded graphites,

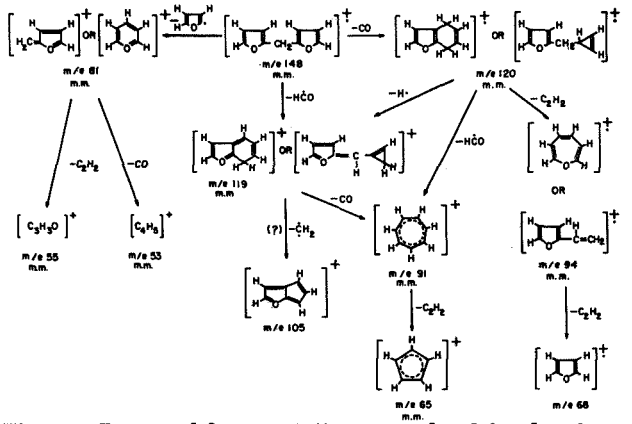

Fig. 3. Proposed fragmentation route for difurylmethane.

and results with the lower-viscosity binders were even better than expected. Where the relatively high electrical resistivity of graphites of this type is acceptable, these are very promising materials.

VI. MASS-SPECTROMETRY STUDIES OF FURFURYL ALCOHOL RESIN COMPONENTS

(E. M. Wewerka, with E. D. Loughran, GMX-2)

A mass-spectrometry study has been made of the behaviors of selected furfuryl alcohol resin components when they are subjected to electron-impact fragmentation. It is hoped that the facility with which the individual components form aromatic molecules when they are fragmented in this way can be related to the ease with which aromatic molecules are produced during thermally induced fragmentation. If this can be done, it may be possible to relate the mass-spectral patterns of furan compounds

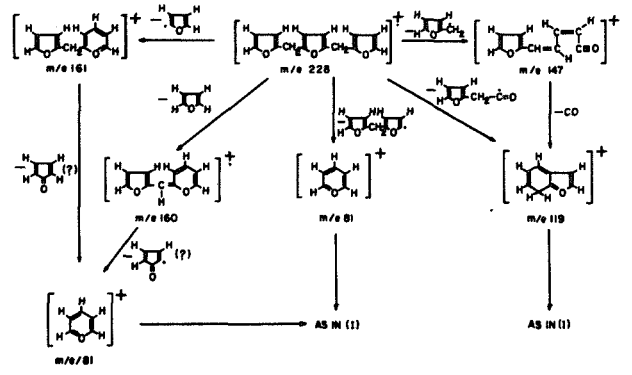

Fig. 4. Proposed fragmentation route for 2,5-difurfuryl-furan.

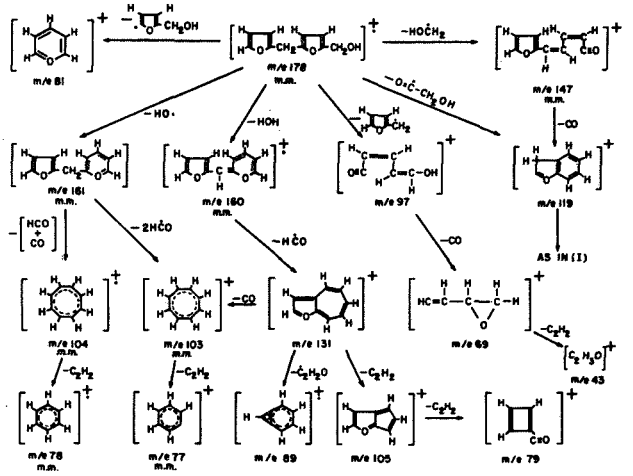

Fig. 5. Proposed fragmentation route for 5-furfuryl-furfuryl alcohol.

directly to the graphitizability of the carbons produced by pyrolyzing them. Among other things, this would provide valuable insight into the components which are most beneficial in furfuryl alcohol resin binders, and thus a useful guide to the synthesis of improved resins.

The electron-impact fragmentation patterns (mass spectra) of six furfuryl alcohol resin components were investigated in detail. These components were: furfuryl alcohol; difurylmethane; difurfuryl ether; 2,5-difurfuryl-furan; 5-furfuryl-furfuryl alcohol; and 4-furfuryl-2-pentenoic acid-γ-lactone. All exhibited rather complicated mass spectra. However, reasonable fragmentation routes have been worked out for all of them, which account quite well for the observed spectra. Five of the proposed fragmentation schemes are shown in Figs. 3-7. That of furfuryl alcohol is not shown because it has previously been reported in detail by J. Collin (Bull. Soc. Chem. Belgium, 69, 575, 1960.)

Although each compound follows many fragmentation routes, those which result in formation of tropylium ion (m/e 91) are of particular interest. This ion is the gas-phase equivalent of the benzyl ion, which we believe to be a main precursor for the formation of other high-molecular-weight aromatic compounds. Other unsaturated aromatic ions (such as the eight-membered rings shown as m/e 103 and 104 in the fragmentation pattern of 5-furfuryl-furfuryl alcohol) could of course also result in

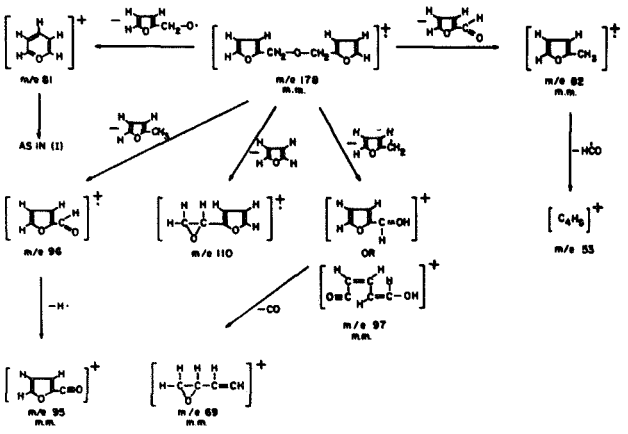

Fig. 6. Proposed fragmentation route for difurfuryl ether.

formation of higher-molecular-weight aromatic compounds. However, ions of this kind are in very low abundance compared to that of the tropylium ion, and therefore are not so far considered to be important.

The percentage of tropylium ions formed by each of the components studied is listed in Table XV. These values are based on the total numbers of fragment ions produced during electron fragmentation. Such molecules as difurylmethane and difurfurylfuran produce large amounts of tropylium ions during fragmentation, while furfuryl alcohol and difurfuryl ether produce relatively few tropylium ions.

Preparative gas chromatography methods are being used to isolate relatively large amounts of each of the components listed in Table XV from the appropriate furfuryl alcohol resins. Each of these will be pyrolyzed, baked, and graphitized, and the structures of the resulting carbons will be characterized. It will thus be determined whether those components which yield the largest amounts of aromatic ions (as typified by the tropylium ion) during electron-impact fragmentation also produce greater abundances of aromatic molecules during pyrolytic decomposition, and more graphitic carbons.

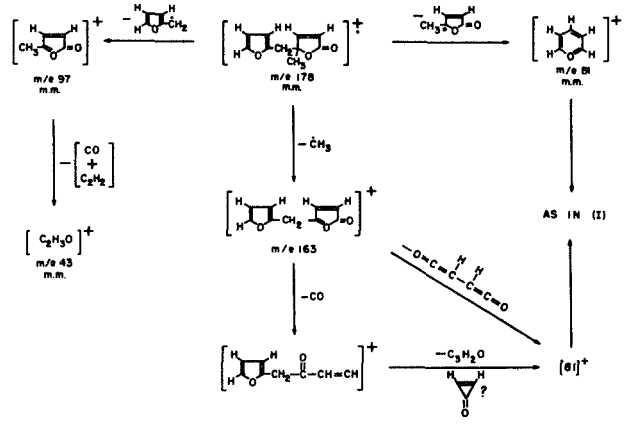

Fig. 7. Proposed fragmentation route for 4-furfuryl-2-pentenoic acid-γ-lactone.

TABLE XV

PROPORTIONS OF TROPYLIUM IONS FORMED BY RESIN COMPONENTS

Component	Percent of Tropylium Ion Produced
Difurylmethane	16
Difurfurylfuran	12
5-Furfuryl-furfuryl alcohol	7
4-Furfuryl-2-pentenoic acid-γ-lactone	2
Difurfuryl ether	0.3
Furfuryl alcohol	0.0

VII. PARTICLE PACKING IN PARTICULATE COMPOSITES

(H. D. Lewis)

A. Previous Work

Particle packing in graphite-matrix composites containing a distribution of ZrC particles was discussed in Report 15 in this series, pp. 23-25. That discussion was concerned with extruded resin-bonded composites made from Lot G-26 Santa Maria graphite flour, a furfuryl alcohol resin binder, and Lot 77D ZrC powder. It was concluded that there was no optimum ZrC addition which would maximize packing efficiency of the graphite filler, but that--at a given ZrC content-- packing might be improved by screening out about 85% of the graphite particles between 40 and 100 μ dia and 90% of the particles coarser than 100 μ dia.

TABLE XVI

INTERVAL-MODEL SAMPLE STATISTICS

FOR GRAPHITE AND ZrC POWDERS

	G-35 Graphite		ZrC
	As Received	-200 # Fraction	Lot 77 D
$\bar{x}_3$	3.190	2.429	2.016
$s^2_{x_3}$	2.476	1.512	0.579
$\bar{x}$	-0.035	0.236	-0.014
s^2_x	0.185	0.176	0.284
$\bar{d}_3$, microns	68.21	20.51	9.67
$s^2_{d_3}$, microns^2	16,120	335.8	44.4
$\bar{d}$, microns	1.10	1.42	1.21
s^2_d, microns^2	0.64	0.91	1.40
g_d	9.69	9.28	8.58
S_W, cm^2/g	3911	5159	1703
CV_d	0.73	0.67	0.98

B. Series ADG Composites

The ADG series of extruded composites discussed in Section IV of this report was made to explore further the effects of ZrC additions on isotropic, high-expansion graphites. The principal filler was Lot G-35 Santa Maria graphite flour, which has been discussed in Section II of this report and is somewhat finer than the Lot G-26 flour, but is otherwise very similar to it. Lot 77D ZrC powder was used, with Varcum 8251 furfuryl alcohol resin binder catalyzed with maleic anhydride.

In this series of composites only the minus 200 mesh fraction of the G-35 graphite flour was used, and the ZrC concentration in the finished composite was varied from 0 to 30 vol %.

Interval-model sample statistics from Micromerograph data are listed in Table XVI for the as-received Lot G-35 graphite flour, for the -200 mesh fraction separated from the G-35 flour for this experiment, and for the ZrC-77D powder. The as-received and -200 mesh graphite flours are further compared with regard to particle-

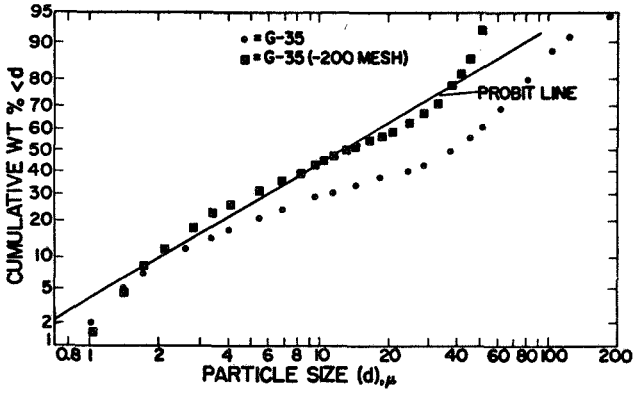

Fig. 8. Log-probability plot of Micromerograph particle-size data for Santa Maria graphite flour, CMB-13 Lot G-35, and for the minus 200 mesh fraction screened from it.

size distribution in Fig. 8, and weight-fraction data for the -200 mesh graphite and the ZrC powders are compared in Fig. 9.

When Fig. 9 is compared with Fig. 13 of Report 15, it appears that the ZrC powder does an even better job of filling the "hole" in the particle-size distribution of the -200 mesh G-35 graphite flour than it did in the case of the Lot G-26 graphite flour previously used. Intuitively it appears that a mix of approximately equal weights of ZrC and -200 mesh G-35 powders would produce a

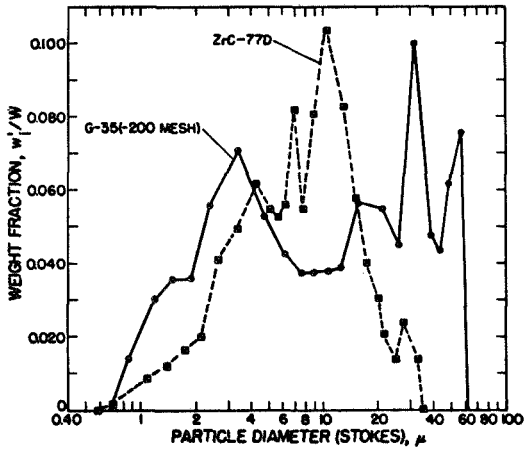

Fig. 9. Weight-fraction diagrams for ZrC-77D and -200 mesh Lot G-35 graphite powders.

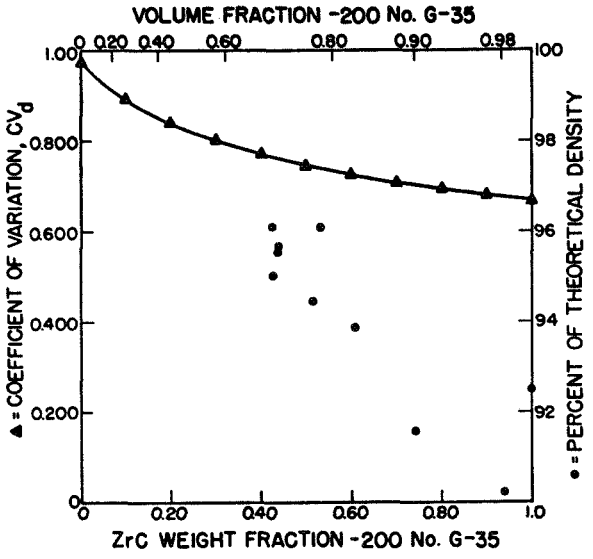

Fig. 10. Calculated coefficient of variation and experimental percent of theoretical density as functions of composite composition in graphite-ZrC composites, Series ADG.

particle-size distribution which was more nearly lognormal than that of the graphite flour alone and had a larger coefficient of variation (CV_d)--both of which would be expected to improve particle packing.

Using the FININT (finite-interval) program, CV_d was calculated for various binary mixtures of the ZrC and graphite powders. These values are plotted in Fig. 10, together with the fraction of theoretical density actually attained in the graphitized composites of the ADG series. Particle-packing efficiency is of course not the only factor that affects the graphitized density of an extruded composite. However, from Fig. 10 it appears that in this case the improvements in particle-size distribution which resulted from ZrC additions to the graphite filler produced a very useful increase in final density of the composite.

VIII. MANUFACTURING PROCEDURES

A. Binder Dilution with Acetone (J. M. Dickinson)

Acetone has been used for a number of years as a mixing aid in our production of graphites and composites bonded with furfuryl alcohol resins. The curing catalyst normally used with such resins has been maleic anhydride, and it has been found convenient to dissolve the catalyst in a small amount of acetone prior to mixing it with the resin. This makes it easier to dissolve the catalyst in the resin and also reduces the viscosity of the resin, which facilities mixing. Low-viscosity resins such as Varcum 8251 (250 cp) can be used successfully either with or without acetone. However, with high-viscosity resins, the reduction in viscosity produced by an acetone addition appears to be useful both in increasing the probability of wetting the surfaces of all filler particles and in permitting the binder to enter their surface-connected porosity. On the other hand, it has also been suggested that copolymerization or other interactions involving the acetone might be damaging to the properties of the graphitized product.

To investigate this possibility, the ADD series of graphites--listed in Tables XVII and XVIII--was made as extruded 0.5-in.-dia rods, using Great Lakes 1008-S graphite flour filler (CMB-13 Lot G-18), three different furfuryl alcohol resin binders, and either three or four levels of acetone concentration. Manufacturing procedures were normal, and final graphitization was to about 2800°C.

The three binders used were: Varcum 8251, a commercial resin with viscosity of 250 cP; QX 247, an experimental Quaker Oats resin (described in Reports 15 and 16 of this series) with viscosity of 880 cP; and EMW 316-317, a CMB-13 experimental resin with viscosity of 1020 cP, discussed above. In each case the acetone and dissolved maleic anhydride were added to a standard amount (189 g) of the binder resin.

Graphites ADD7 through ADD10 and graphite ADD15 were all made with the low-viscosity Varcum 8251 furfuryl alcohol resin. Acetone additions to the resin produced no significant changes in bulk density, electrical resistivity, or Young's modulus of the finished graphite. In the manufacture of rod ADD8 the blended mix was stored in a covered bowl for one week before it was chopped and extruded, to permit the binder to "soak into" the filler particles. This produced a significant increase in density of the final product, which was reflected in its other properties. A similar effect has previously been

TABLE XVII

ADD GRAPHITES, EXTRUSION CONDITIONS

Specimen Number	Binder	Acetone Added, (a) mℓ	Extrusion Conditions					Green Dia. in.
			Pressure, psi	Velocity, in./min	Vacuum, Torr	Temperature, °C Mix	Temperature, °C Chamber	
ADD 7	Varc. 8251	0	4590	164	1000	40	45	0.506
ADD 15	Varc. 8251	15	4860	160	<1000	38	48	0.506
ADD 8 (b)	Varc. 8251	15	7650	171	700	42	45	0.5025
ADD 9	Varc. 8251	30	5310	154	800	40	42	0.507
ADD 10	Varc. 8251	60	5130	167	600	38	48	0.507
ADD 1	QX 247	0	7650	157	700	35	70	0.5025
ADD 5	QX 247	0	6120	157	600	39	43	0.5035
ADD 2	QX 247	10	6300	164	900	35	46	0.503
ADD 3	QX 247	20	5850	171	600	41	50	0.503
ADD 4	QX 247	40	6840	171	500	41	44	0.503
ADD 6	QX 247	80	5625	164	600	38	40	0.5045
ADD 11	EMW 316-317	0	5940	164	200	45	45	0.504
ADD 12	EMW 316-317	15	5940	171	<500	44	45	0.504
ADD 13	EMW 316-317	30	5400	171	<500	44	45	0.504
ADD 14	EMW 316-317	60	6750	150	<400	42	45	0.5035

(a) To 189 g binder.

(b) Blended mix held 1 week before extruding.

observed for mixes stored a day or two before extruding, although to a lesser degree. This behavior is further discussed in the next section of this report.

Graphites ADD1 through ADD6 were made with the intermediate-viscosity QX247 resin. Densities are lower than would be expected for this filler-binder combination, which has been traced to a poorer vacuum than usual in the baking furnace. Some oxidation occurred during baking, and the absolute values of properties listed for these graphites are therefore not representative. However, relative values within the group are believed to be significant, and show no important variation with the proportion of acetone added to the binder.

An experimental CMB-13 resin, EMW 316-317, with viscosity slightly higher than that of QX247, was used to make rods ADD11 through ADD14. These were all high-density graphites with good properties. Again there was no trend of properties with the proportion of acetone added.

It has been concluded that acetone is a useful mixing addition to furfuryl alcohol resin binders, and that it can and should be used to simplify and improve the manufacturing process when these binders are used. It decreases binder viscosity to a desirable degree, making mixing operations faster, easier, and more effective. It assists in distributing the maleic anhydride catalyst uniformly, accelerating curing. Its use appears to have no significant effect on the properties of the final product and, if it is used in reasonable amounts, it is believed that the acetone is in fact essentially completely removed from the mix during the chopping and preliminary extrusion operations routinely used here in advance of final extrusion.

B. Soaking-in of the Binder (J. M. Dickinson)

As has been described above, it has been observed that when a resin-bonded mix was stored for a few days before extrusion the binder appeared to soak into the

TABLE XVIII

PROPERTIES OF ADD GRAPHITES

Specimen Number	Acetone Added, mℓ	Bulk Density, g/cm^3	Binder Carbon Residue, %	Electrical Resistivity, μΩcm	Young's Modulus, 10^6 psi
ADD 7	0	1.869 ± 0.002	45.5 ± 0.3	1138 ± 8	2.36 ± .02
ADD 15	15	1.874 ± 0.002	---------	1137 ± 9	2.40 ± 0.01
ADD 8[(a)]	15	1.899 ± 0.003	47.1 ± 0.2	1079 ± 9	2.56 ± .01
ADD 9	30	1.867 ± 0.004	46.1 ± 0.3	1150 ± 12	2.36 ± .03
ADD 10	60	1.871 ± 0.004	45.8 ± 0.2	1135 ± 5	2.37 ± .03
ADD 5	0	1.856 ± 0.008	47.8 ± 0.2	1118 ± 6	2.71 ± 0.06
ADD 2	10	1.854 ± 0.003	47.8 ± 0.2	1116 ± 11	2.69 ± 0.05
ADD 3	20	1.850 ± 0.003	47.4 ± 0.1	1127 ± 18	2.67 ± 0.06
ADD 4	40	1.851 ± 0.002	48.0 ± 0.3	1130 ± 6	2.67 ± 0.06
ADD 6	80	1.856 ± 0.004	46.9 ± 0.3	1150 ± 22	2.59 ± 0.04
ADD 11	0	1.916 ± 0.003	49.0 ± 0.3	1092 ± 13	2.68 ± 0.03
ADD 12	15	1.922 ± 0.002	49.5 ± 0.2	1071 ± 8	2.66 ± 0.03
ADD 13	30	1.912 ± 0.003	48.6 ± 0.4	1076 ± 6	2.61 ± 0.01
ADD 14	60	1.921 ± 0.004	49.6 ± 0.1	1077 ± 6	2.67 ± 0.02

(a) Blended mix held 1 week before extruding.

filler, and the result was an increase in the density and other properties of the finished graphite. To examine this effect, graphite ADK1 was made from 85 parts G-18 (Great Lakes 1008 -S) graphite flour and 15 parts Thermax carbon black, using Varcum 8251 furfuryl alcohol resin binder catalyzed with maleic anhydride. After twin-shell blending the raw mix was stored for one week in a bowl covered with aluminum foil. It was weighed daily, and no weight change was observed to occur, indicating that the foil cover kept the vapors from the binder in contact with the mix. It was then extruded at 164 in./min, the mix and chamber temperatures being 45 and 40°C respectively and the chamber vacuum 1000 torr. Extrusion pressure was higher than usual for a mix of this type, and green diameter was 0.504 in. Curing, baking, and graphitizing cycles were normal.

Density of the finished graphite was 1.894 g/cm^3, compared with 1.87 to 1.88 g/cm^3 for similar graphites extruded immediately after mixing. Electrical resistivity (1128 μΩcm) was a little lower than usual, and Young's modulus (2.55 x 10^6 psi) was a little higher than usual.

Although further experiments are needed to determine the effects of temperature, time, pressure, and atmosphere, it appears that simply storing the resin-bonded raw mix for a few days before extruding it significantly improves the properties of the finished graphite. This is assumed to result from slow absorption of the binder into the surface-connected porosity of the filler.

IX. MECHANICAL PROPERTIES

A. Young's Moduli of POCO Graphites (P. E. Armstrong)

Dynamic Young's modulus has been measured as a function of temperature over the range 25 to 1800°C for each of six samples of POCO graphites of various densities, each of which had been annealed for 1/2 hr at 2900°C. At each of a series of temperatures in this range, Young's modulus was plotted as a function of fractional porosity, as has previously been done with data obtained at room temperature. Fractional porosity

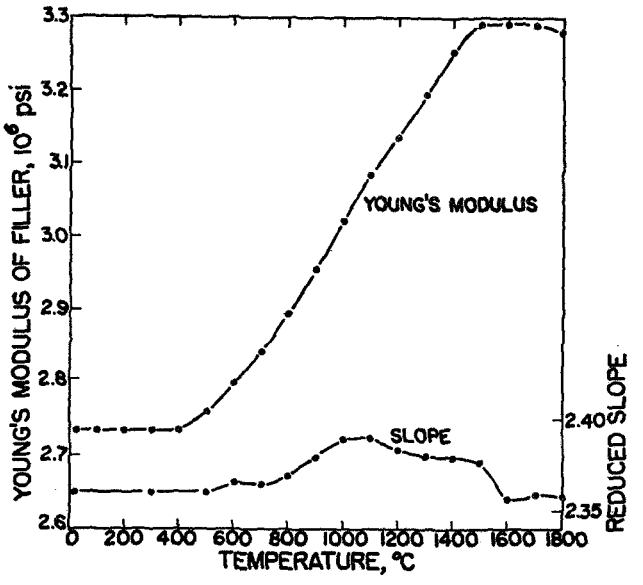

Fig. 11. Effects of temperature on Young's modulus of the POCO filler and on the reduced slope of the Young's modulus vs fractional porosity curve at a given temperature.

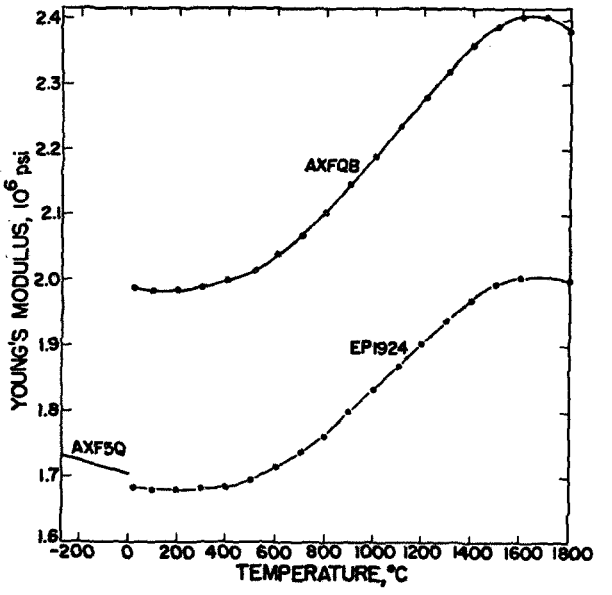

Fig. 12. Effects of temperature on the dynamic Young's moduli of three grades of POCO graphite.

at the elevated temperature was calculated as unity minus the ratio of bulk density to crystallite density at that temperature. Bulk density at temperature was calculated from that determined at room temperature and the measured bulk thermal expansion of the sample. Crystallite density at temperature was calculated from an assumed room-temperature value of 2.25 g/cm^3 and literature values for the thermal expansion of single-crystal graphite.

At all temperatures in the range investigated, Young's modulus was found to decrease linearly with increasing fractional porosity. At each temperature the plot of modulus vs fractional porosity was extrapolated to a porosity value equivalent to an assumed room-temperature bulk density of 2.15 g/cm^3. The modulus value at that porosity was assumed to represent the Young's modulus of the filler, uncomplicated by the effects of any interparticle porosity. In Fig. 11 Young's modulus of the filler, derived in this way, has been plotted as a function of temperature, together with the "reduced slope" of the modulus vs porosity curve at the same temperature. Reduced slope was calculated by determining the actual slope of the modulus vs porosity curve at a given temperature and dividing it by the corresponding value of filler-particle modulus (determined by extrapolation).

Reduced slope should be independent of changes in temperature and in properties of the filler material, varying only with changes in the nature of the interparticle porosity. In fact, it is shown in Fig. 11 to increase slightly in the temperature region in which Young's modulus of the filler is increasing most rapidly. However, the maximum increase is only about 1%, so that the effect of changes in the interparticle porosity on the Young's modulus vs temperature relation is believed to be small. If the relatively large increase in Young's modulus of the filler between about 400 and 1400°C is due to a change in porosity, it is evidently the internal porosity of the filler particles that is principally involved.

Figure 12 shows the Young's modulus vs temperature behavior of two POCO grades of quite different density: Grade AXFQB, with bulk density of 1.906 g/cm^3, and Grade EP1924, with bulk density of 1.801 g/cm^3. The two curves are nearly parallel, with the higher-density

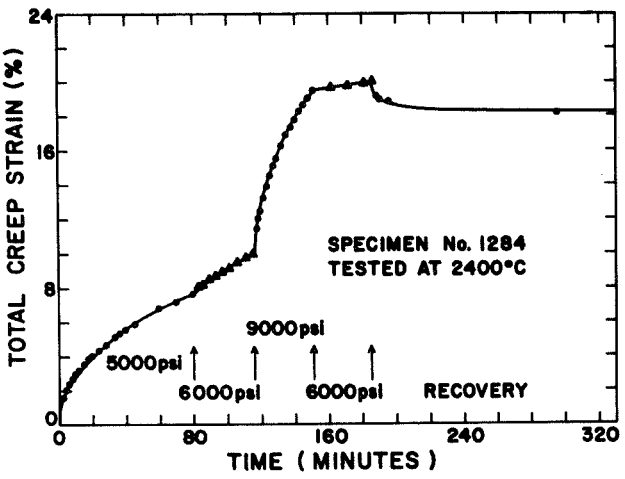

Fig. 13. Creep curve for a test embodying several stress changes and a recovery period under zero load.

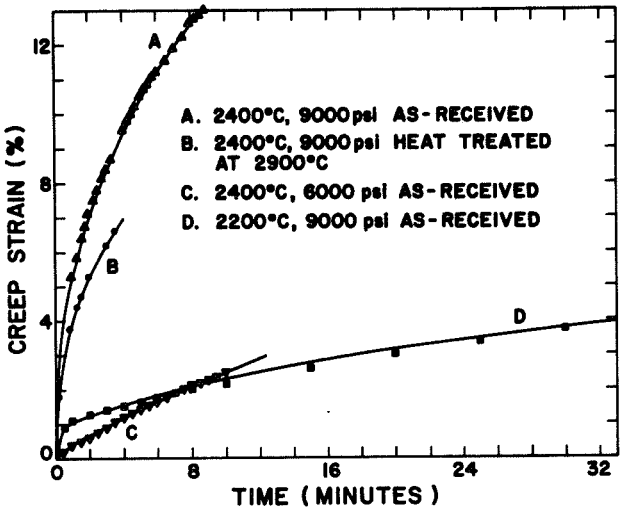

Fig. 14. Initial portions of creep curves for several different test conditions.

graphite having a modulus about 0.3 to 0.4 x 10^6 psi higher at all temperatures.

Another sample of POCO graphite (Grade AXF5Q, with room-temperature bulk density of 1.824 g/cm^3) was available whose dimensions were suitable for dynamic modulus measurements in a helium cryostat. In Fig. 12 its dynamic Young's modulus is plotted between 0° and -269°C (4°K). Over this temperature interval its modulus increased only 1.6%.

The bulk thermal expansions of all six POCO graphite samples were essentially identical over the temperature range 25 to 1800°C. This agrees with results discussed in Reports 15 and 16 in this series, which also indicated that the thermal expansion coefficients of annealed POCO graphites were independent of their bulk densities.

B. Creep Behavior of a POCO Graphite (E. G. Zukas, W. V. Green)

The tensile creep behavior of POCO Grade HPD-1 graphite has been investigated over the temperature range 2200 to 2500°C. The material tested was purchased from the manufacturer as 3/4-in.-dia rods, whose average bulk density was 1.84 g/cm^3. Creep measurements were made on the graphite as-received and after annealing it at 2750°C and at 2900°C. Cylindrical specimens were used, with gauge sections 0.220-in. dia and 1-in. long. These were tested in an argon atmosphere in a constant-force testing machine, with optical measurements of both strain and temperature.

The apparent activation energy for creep, Q_c, and the stress exponent of the creep rate, n, were determined from temperature-cycling and stress-cycling experiments. Strain recovery was observed by measuring the spontaneous shortening of the specimen which occurred with time at the creep temperature after the creep load was removed. Volume changes were determined by measuring the dimensions of the specimen gauge sections at room temperature before and after creep. The microstructural changes accompanying creep were investigated by preparing flat surfaces on special specimens, protecting them during creep by wrapping the specimens in prebaked pyrolytic graphite tape, testing them in an atmosphere of spectroscopic-grade argon, and examining the same areas by optical and electron microscopy before and after the creep test.

The creep behavior observed in a typical test is illustrated in Fig. 13, which is for an as-received HPD-1 specimen tested in tension at 2400°C. The decrease in creep rate with increasing strain, referred to as "work-hardening," is typical of polycrystalline graphites as well as many other materials. The large increase in creep rate resulting from a modest increase in stress indicates a strong stress-dependence of the creep rate,

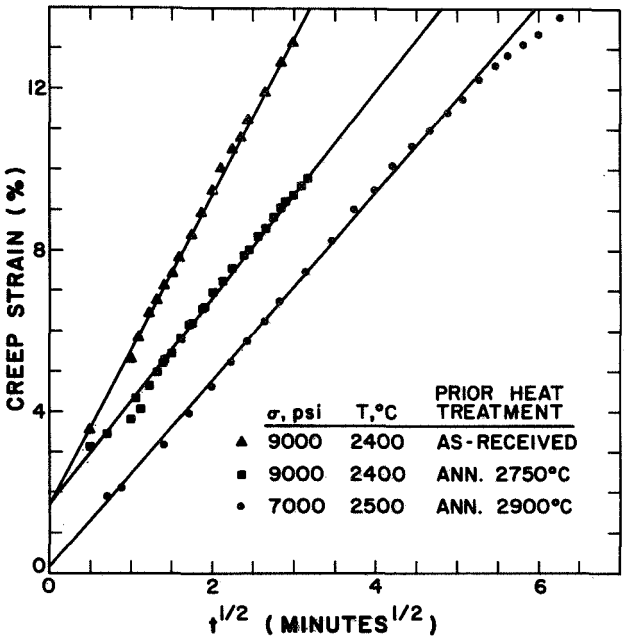

Fig. 15. Creep strain as a function of $t^{\frac{1}{2}}$ for POCO HPD-1 graphite as-received and after heat-treatment at 2750 and 2900°C.

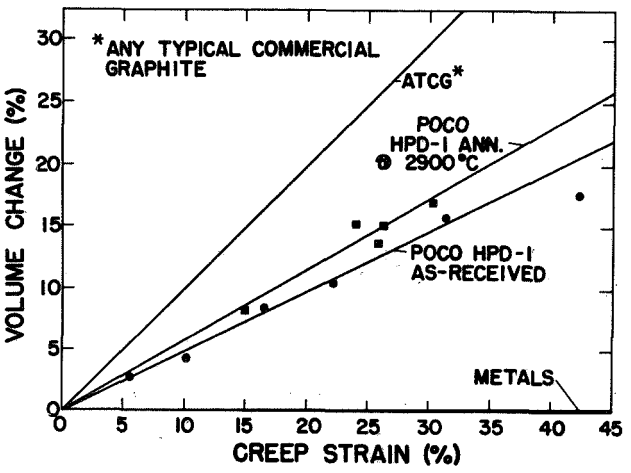

Fig. 16. The volume change in the sample gauge section as a function of creep strain for a typical manufactured graphite, a typical metal, and POCO HPD-1 graphite.

which is also typical of graphites. Strain-recovery after removal of the creep load is initially very rapid, but the rate of recovery decays almost to zero in a relatively short time.

The initial portions of several different creep curves are shown in Fig. 14. The general effects of prior heat treatment, stress, and temperature are apparent.

Creep strain, ε_c, was found to increase with time, t, approximately according to the transient time law,

$$\varepsilon_c = A t^b ,$$

where A and b are constants. As has been true for a large number of other manufactured graphites, the best value determined for the exponent b was $b = \frac{1}{2}$. Figure 15 demonstrates that, for HPD-1 graphite, ε_c increases in direct proportion to $t^{\frac{1}{2}}$ for the heat-treated as well as for the as-received material, and at a variety of stresses and temperatures. It also illustrates the structural instability of the as-received material which, at 2400°C and 9000 psi, had a creep rate significantly higher than did material heat-treated at 2750°C before testing under these same conditions.

When metals are extended in tensile creep, the volume change in the gauge section is essentially zero. When typical manufactured graphites are similarly tested, the cross-sectional area of the gauge section remains essentially constant, the macroscopic axial strain being accounted for by a volume increase produced by the opening of internal cracks and voids. As is illustrated by Fig. 16, the behavior of a POCO graphite is intermediate between these extremes. Examination of the same areas by optical and scanning-electron microscopy before and after straining demonstrated both the expected longitudinal extension and the lateral contraction of the material locally, and increases in both the lengths and the widths of preexisting voids. Some new porosity developed as strain increased, but no evidence was found of the cleavage cracks which normally develop in a manufactured graphite as it is strained in tension. Evidently the normal deformation mode of a polycrystalline graphite--the opening of voids--occurs in POCO HPD-1 graphite, but in the temperature range investigated this was accompanied by real plastic deformation instead of local cleavage.

These results show both similarities and differences between the creep behaviors of POCO HPD-1 graphite and those of other manufactured polycrystalline graphites. In particular:

1. The apparent activation energy for tensile creep of HPD-1 graphite, Q_c, was 230 ± 30 kcal/mole for the as-received material, and increased to 250 ± 20 kcal/mole for the same material annealed to 2900°C before testing. (Although this "increase" was within the uncertainty of the determination, it is believed to be real.) Values previously determined for other commercial graphites have normally been about 250 ± 20 kcal/mole. Since this is essentially the activation energy for self-diffusion in graphite, the creep rate appears to be diffusion-controlled in HPD-1 graphite as well as in other manufactured graphites.

2. For HPD-1 graphite, the exponent n, representing stress-dependence of the tensile creep rate, was about 5 for the as-received material, but increased to about 8 for material annealed to 2900°C. For most other commercial graphites it is in the range 6 to 8.

3. For HPD-1 as for a large number of other graphites, the exponent b, representing the time dependence of the tensile creep rate, was 1/2.

4. The shape of the tensile creep curve of HPD-1 graphite is similar to that of other commercial graphites, showing "work hardening", i.e., a creep rate which decreases as strain increases.

5. Tensile creep strains to fracture are large for HPD-1 graphite, generally exceeding 30%. By careful control during testing they can be made to exceed 70%. For most other commercial graphites, creep strain to fracture in this temperature region is in the range 2 to 10%.

6. During tensile creep deformation, the cross-sectional area of an HPD-1 graphite specimen decreases by as much as 20%. For most other commercial graphites, the cross-sectional area remains essentially constant during creep extension.

7. The volume of HPD-1 graphite increases as it is extended in tensile creep, but to an extent only about one-half that observed for other commercial graphites.

8. The macroscopic strain of HPD-1 graphite in tensile creep is accomplished in part by opening of preexisting voids, as is the case in other commercial graphites, but appears also to involve real plastic deformation instead of the general microcracking normally observed in other graphites.

9. Recovery of tensile creep strain (shortening of the specimen after the creep load is removed) occurs normally in HPD-1, but eliminates only about 10% of the total creep strain, compared to 25 to 35% (of a much smaller total strain) for other commercial graphites.

10. Tensile fracture stresses for HPD-1 graphite are very high in the temperature range 2200 to 2500°C, sometimes reaching 18,000 to 20,000 psi. However, creep occurs at stresses much lower than the fracture stresses. Thus at 2400°C a stress one-third of that required to fracture the material will cause it to creep at a significant rate.

11. As it is received from the manufacturer, HPD-1 graphite appears to be structurally unstable. Annealing it at such temperatures as 2750°C or 2900°C reduces both its creep rate under a given tensile load and the amount of tensile strain it sustains in advance of fracture. Holding it at a lower temperature (e.g., 2400°C) after it has been strained has similar effects.

X. THERMOPHYSICAL PROPERTIES

(P. Wagner)

A. Thermal Expansion of Pyrolytic Graphite Tubes

Measurements have been made of the linear thermal expansion in both the radial and the axial directions of three pyrolytic graphite tubes constituting a nested set intended for use as a high-temperature thermal insulator. Between room temperature and 645°C the expansion measurements were made in a quartz dilatometer.

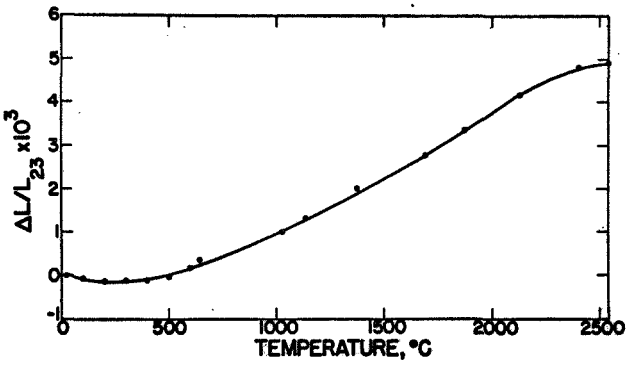

Fig. 17. Linear thermal expansion of the outer pyrolytic graphite tube, measured parallel to the tube axis.

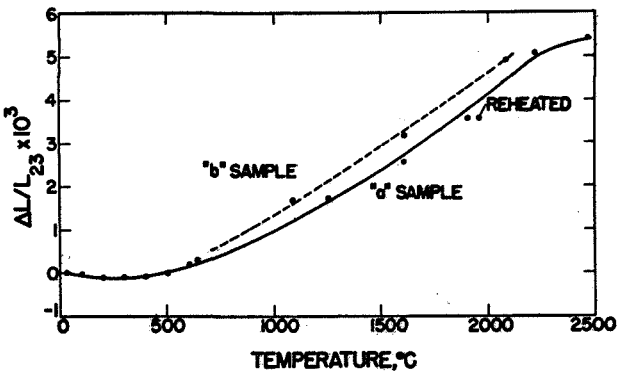

Fig. 18. Linear thermal expansion of two samples from the intermediate pyrolytic graphite tube, measured parallel to the tube axis.

Between about 1000 and about 2500°C an optical technique was used. All measurements were made in an argon atmosphere.

Specimens to be used for axial expansion measurements were cut parallel to the tube axis, and were necessarily thin enough to introduce the danger of buckling in the push-rod dilatomer. Specimens for radial measurements were made by stacking thin (0.18 cm thick) sections cut from the tube walls either in a holder or suspended as a stack, offering the possibility of component hang-up or rotation when the stack was suspended in the high-temperature furnace. It was therefore expected that for the axial specimens the results would be more reliable in the higher-temperature experiments, while for the radial measurements the greater reliability would be in the low-temperature range. However, no obvious difficulties arose from these sources, and the apparent matching of high- and low-temperature data in all cases indicates that sample configuration is probably not the limiting factor with regard to validity of the results.

Data obtained in these experiments are plotted in Figs. 17 through 22 as curves of fractional change in length, $\Delta L/L_{23}$, vs temperature for each of the three tubes in both orientations. The first three of these curves illustrate the initial contraction expected for directions within the layer planes of a well-oriented graphite. All six curves show a decrease in the temperature-rate of thermal expansion above about 2000°C, which is probably associated with improvements in the graphite structure produced by heating.

Samples of this pyrolytic graphite in the original and the posttest conditions were examined with the optical microscope by R. D. Reiswig, CMB-13; with the electron microscope by L. S. Levinson, CMB-13; and by x-ray diffraction by J. A. O'Rourke, CMB-13. It was observed that the tubes had been manufactured by depositing carbon on the inside of a larger tube rather than on the outside of a mandrel. The pyrolytic graphite was not entirely "continuously nucleated;" some of the growth cones extended almost or entirely through the thickness of the tube wall. Local delaminations occurred, but they were not extensive in either the original or the posttest condition. Ion-bombardment etching developed grooves parallel to basal planes in the case of tested pieces but not

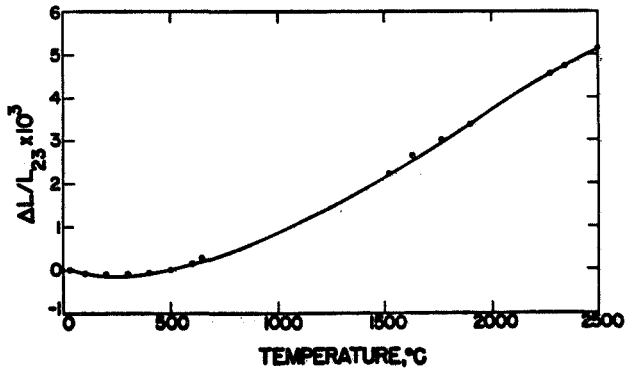

Fig. 19. Linear thermal expansion of the inner pyrolytic graphite tube, measured parallel to the tube axis.

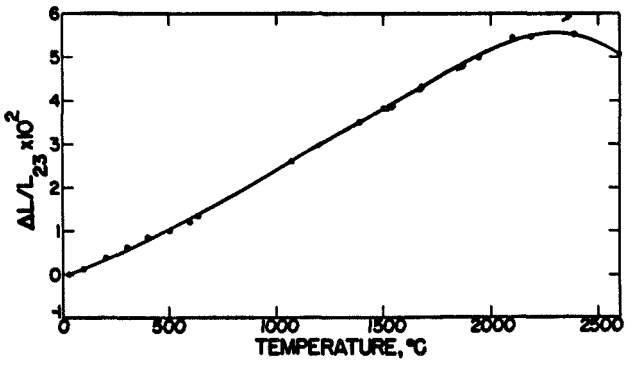

Fig. 20. Linear thermal expansion of the outer pyrolytic graphite tube, measured normal to the tube axis. A second run is indicated by the arrows.

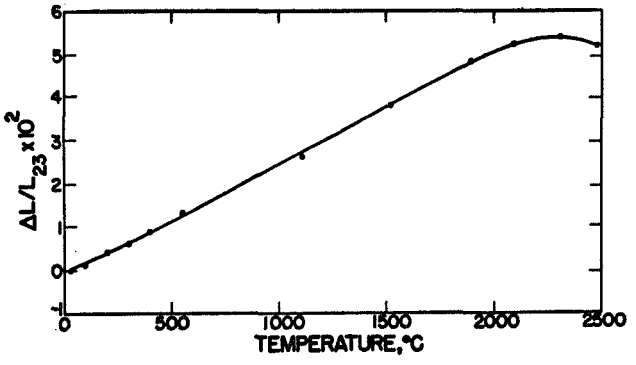

Fig. 22. Linear thermal expansion of the inner pyrolytic graphite tube, measured normal to the tube axis.

in the case of untested ones, a change in behavior which normally occurs when pyrolytic graphite has been heated sufficiently to improve its crystal structure. X-ray measurements gave L_c values of 177 and 182Å for the original and tested conditions respectively, and corresponding d_{002} values of 3.422 and 3.417 Å, indicating a small improvement in crystallinity as a result of heating. The degree of preferred orientation was also increased by heating, the M value (from $I = I_o \sin^M \Phi$) increasing from 8.8 to 9.6 and the Bacon Anisotropy Factor (σ_{oz}/σ_{ox}) increasing from 9.7 to 10.9.

During the course of these experiments each of the axial specimens developed a bow, outward from the tube axis, whose height was 3 to 6.4 mm in a specimen length of about 65 mm. Each of the specimens also increased permanently in length by about 0.2%, probably as a result of layer-plane de-wrinkling accompanying the graphitization described above. As is illustrated in Fig. 18, when the "a" sample of the intermediate tube was run to 2469°C, cooled, and then reheated to 1962°C, the expansion value measured at 1962°C fell below the curve representing the first heating of the sample. This suggested hysteresis in the sample's thermal expansion. A second ("b") sample was therefore tested, its dilatation during the first heating following the dashed curve of Fig. 18. After heating to 2574°C it was cooled, then reheated to 1167°C, where a measurement was made. The point representing this measurement fell on the solid curve representing the "a" sample, well below the dashed line representing the behavior of the "b" sample during its first heating. This reduction in thermal expansion after the first cycle of heating to a relatively high temperature probably results jointly from improvement in the layer-plane structure and from better alignment of the layer planes with the axial direction of the tube, which is the direction in which these measurements were made.

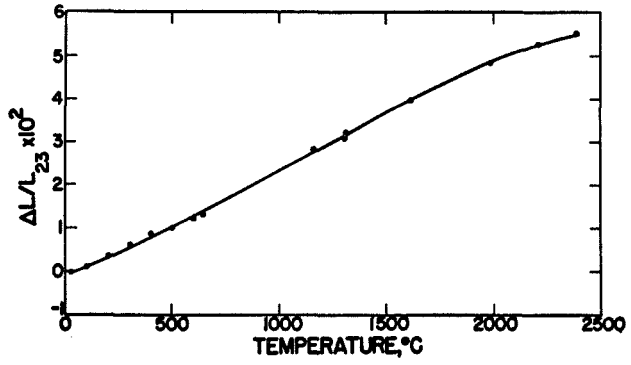

Fig. 21. Linear thermal expansion of the intermediate pyrolytic graphite tube, measured normal to the tube axis.

The heating and cooling cycle involved in these experiments caused the stacked radial specimens to decrease in overall length by an average 2.5%. As was observed for the longitudinal samples, the thermal-expansion coefficient in the radial direction decreased during heating above about 2000°C. For the radial specimens this was not due to improvements in the crystal structure and preferred orientation of the graphite, both of which would increase thermal expansion in the

TABLE XIX

MEASURED THERMAL DIFFUSIVITIES

AND CALCULATED THERMAL CONDUCTIVITIES OF GRAPHITE-ZrC COMPOSITES

Material	ZrC Content, Vol. %	Direction of Measurement	Thermal Diffusivity, α, cm^2/sec	Thermal Conductivity, λ, W/cm-K
ACP-18	0.16	With-grain	0.82	1.10
		Across-grain	0.50	0.67
ACP-17	0.31	With-grain	0.76	1.01
		Across-grain	0.51	0.68
ACP-16	0.62	With-grain	0.80	1.07
		Across-grain	0.49	0.66
ACP-6	4.67	With-grain	0.76	1.04
		Across-grain	0.50	0.69
ACP-8	9.07	With-grain	0.69	1.11
		Across-grain	0.45	0.73
ACP-13	17.2	With-grain	0.66	0.99
		Across-grain	0.45	0.67

direction in which the measurements were made. It apparently resulted from the permanent dimensional changes caused by decreases in interlayer spacing (d_{002}) and by de-wrinkling of the layer planes. It would therefore be expected that, after the first cycle of heating to a graphitizing temperature, these dimensional changes would not be repeated during subsequent reheating to lower temperatures, and that the coefficient of thermal expansion would be smaller at the lower temperatures but would continue to increase at the higher temperatures. As is illustrated by the arrows in Fig. 20, a radial specimen of the outer pyrolytic graphite tube was thermally cycled. At least up to 2355°C (represented by the final arrow) there was no noticeable fall-off at the higher temperatures in the rate of thermal expansion during the second heating. At lower temperatures, however, the expected decrease in thermal expansion coefficient did not occur.

B. Thermal Diffusivities of Graphite-ZrC Composites

The manufacture and some of the properties of the ACP series of graphite-matrix, graphite-ZrC composites were discussed in Reports 14 and 15 in this series. Room-temperature thermal-diffusivity measurements have since been made on the six composites from this series listed in Table XIX, which ranged in ZrC content from 0.16 to 17.25 volume %. Thermal conductivities (λ) were computed from the diffusivity values (α) using the relation

$$\lambda = (W_{ZrC} C_{P_{ZrC}} + W_G C_{P_G}) \alpha \rho_{measured}$$

where W and C_P represent weight fraction and heat capacity, respectively, the subscripts identify ZrC and graphite, and ρ is the measured density of the composite.

From Table XIX, it is clear that the thermal diffusivity of a graphite-ZrC composite decreases as its concentration of ZrC increases. The effect of changing ZrC concentration on thermal conductivity, if any, is far less pronounced. This difference in the trends of α and λ is to be suspected in multicomponent systems in which the components differ in volume heat capacity.

XI. PUBLICATIONS RELATING TO CARBONS AND GRAPHITES

Powell, R. L. and Wagner, P., "Irradiation Effects on Low Temperature Thermal and Electrical Conductivities of two Graphites," Letter-to-the-Editor, Carbon, Vol. 8, pp. 692-693, 1970.

Smith, M. C., "CMB-13 Research on Carbon and Graphite, Report No. 16, Summary of Progress from November 1, 1970 to January 31, 1971," LA-4714-MS, July, 1971.

Wewerka, E.M., Loughran, E. D. and Walters, K. L., "Study of the Low Molecular Weight Components of Furfuryl Alcohol Polymers," J. Appl. Polymer Sci., V. 15, pp. 1437-51, 1971.

Zukas, E. G. and Green, W. V., "Creep Behavior of Hot Isostatically Pressed Graphite," Carbon, Vol. 9, No. 3, pp. 341-344, 1971.

EE, ALT/gc:124(90)